

# Dissipationless Quantum Spin Current at Room Temperature

Shuichi Murakami,<sup>1\*</sup> Naoto Nagaosa,<sup>1,2,3</sup> Shou-Cheng Zhang<sup>4</sup>

Although microscopic laws of physics are invariant under the reversal of the arrow of time, the transport of energy and information in most devices is an irreversible process. It is this irreversibility that leads to intrinsic dissipations in electronic devices and limits the possibility of quantum computation. We theoretically predict that the electric field can induce a substantial amount of dissipationless quantum spin current at room temperature, in hole-doped semiconductors such as Si, Ge, and GaAs. On the basis of a generalization of the quantum Hall effect, the predicted effect leads to efficient spin injection without the need for metallic ferromagnets. Principles found here could enable quantum spintronic devices with integrated information processing and storage units, operating with low power consumption and performing reversible quantum computation.

Our work is driven by the confluence of the important technological goals of quantum spintronics (1, 2) with the quest of generalizing the quantum Hall effect (QHE) to higher dimensions. The QHE is a manifestation of quantum mechanics observable at macroscopic scales. In contrast to most transport coefficients in solid-state systems, which are determined by the elastic and the inelastic scattering rates, the Hall conductance  $\sigma_H$  in QHE is quantized and completely independent of any scattering rates in the system, where the transport equation is given by  $j_\alpha = \sigma_H \epsilon_{\alpha\beta} E_\beta$  [ $j_\alpha$  and  $E_\beta$  ( $\alpha, \beta = 1, 2$ ) are the charge current and the electric fields respectively,  $\epsilon_{\alpha\beta}$  is the fully antisymmetric tensor in two dimensions]. Though dissipative transport coefficients are expressed in terms of states in the vicinity of the Fermi level, the nondissipative quantum Hall conductance is expressed in terms of equilibrium response of all states below the Fermi level. The topological origin of the QHE is revealed through the fact that the Hall conductance can also be expressed as the first Chern number of a  $U(1)$  gauge connection defined in momentum space (3). Recently, the QHE has been generalized to four spatial dimensions (4). In that case, an electric field  $E_\nu$  induces an  $SU(2)$  spin current  $j_\mu^i$  ( $\mu, \nu = 1, 2, 3, 4$ ,  $i = 1, 2, 3$ ) through the nondissipative transport equation  $j_\mu^i = \sigma \eta_{\mu\nu}^i E_\nu$ , where  $\eta_{\mu\nu}^i$  is the 'tHooft tensor, explicitly given by  $\eta_{\mu\nu}^i = \epsilon_{i\mu\nu 4} + \delta_{i\mu} \delta_{4\nu} - \delta_{i\nu} \delta_{4\mu}$ , and  $\sigma$  is a dissipa-

tionless transport coefficient. The quantum Hall response in that system is physically realized through the spin-orbit coupling in a time-reversal symmetric system. At the boundary of this four-dimensional quantum liquid, when both the electric field and the spin current are restricted to the three-dimensional sub-space, the dissipationless response is given by

$$j_j^i = \sigma_s \epsilon^{ijk} E_k \quad (1)$$

This fundamental response equation shows that it is possible to induce a purely topological and dissipationless spin current by an electric field in the physical, three-dimensional space.

We consider a realization of this electric field-induced topological spin current in conventional hole-doped semiconductors. In a large class of semiconductors, including Si, Ge, GaAs, and InSb, the valence bands are fourfold degenerate at the  $\Gamma$  point (Fig. 1). The effective Luttinger Hamiltonian (5) for holes is given by

$$H_0 = \frac{\hbar^2}{2m} \left( \left( \gamma_1 + \frac{5}{2} \gamma_2 \right) k^2 - 2\gamma_2 (\mathbf{k} \cdot \mathbf{S})^2 \right) \quad (2)$$

where  $S_i$  is the spin-3/2 matrix. We take the hole picture, and reverse the sign of the energy. Good quantum numbers for this Hamiltonian are the helicity  $\lambda = \hbar^{-1} \mathbf{k} \cdot \mathbf{S} / k$  and the total angular momentum  $\mathbf{J} = \hbar \mathbf{x} \times \mathbf{k} + \mathbf{S}$ . This kinetic Hamiltonian is diagonalized in the basis where the helicity operator  $\lambda$  is diagonal and the eigenvalue is given by

$$\epsilon_\lambda(\mathbf{k}) = \frac{\hbar^2 k^2}{2m} \left( \gamma_1 + \left( \frac{5}{2} - 2\lambda^2 \right) \gamma_2 \right) \equiv \frac{\hbar^2 k^2}{2m_\lambda}$$

For a given wave vector  $\mathbf{k}$ , the Hamiltonian (Eq. 2) has two eigenvalues,

$$\epsilon_H(\mathbf{k}) = \epsilon_{\lambda=\pm 3/2}(\mathbf{k}) = \frac{\gamma_1 - 2\gamma_2}{2m} \hbar^2 k^2 \equiv \frac{\hbar^2 k^2}{2m_H}$$

and

$$\epsilon_L(\mathbf{k}) = \epsilon_{\lambda=\pm 1/2}(\mathbf{k}) = \frac{\gamma_1 + 2\gamma_2}{2m} \hbar^2 k^2 \equiv \frac{\hbar^2 k^2}{2m_L}$$

forming Kramers doublets. They are referred to as the light-hole (LH) and heavy-hole (HH) bands. In semiconductors with zincblende structure, such as GaAs, inversion symmetry breaking causes an additional tiny splitting in the LH and HH bands. We can neglect the inversion symmetry breaking when the temperature is much higher than this splitting. The band structure of semiconductors deviates from the spherical to the cubic symmetry. We also neglect this effect for simplicity, because physics described below are not so much affected by it.

We shall consider the effect of a uniform electric field  $\mathbf{E}$ . Our full Hamiltonian is thus given by  $H = H_0 + V(\mathbf{x})$ , where  $V(\mathbf{x}) = e\mathbf{E} \cdot \mathbf{x}$ , and  $-e$  is the charge of an electron. We assume that the split-off band is totally occupied. We first define a 4 by 4 unitary matrix  $U(\mathbf{k})$  which diagonalizes the kinetic Hamiltonian  $H_0$ .  $U(\mathbf{k})$  is defined by  $U(\mathbf{k})(\mathbf{k} \cdot \mathbf{S}) U^\dagger(\mathbf{k}) = k S_z$ . In the spherical coordinates where  $\mathbf{k} = k(\sin\theta\cos\phi, \sin\theta\sin\phi, \cos\theta)$ ,  $U(\mathbf{k})$  can be expressed as  $U(\mathbf{k}) = \exp(i\theta S_y) \exp(i\phi S_z)$ . Under this unitary transformation, the new Hamiltonian  $\tilde{H} \equiv U(\mathbf{k}) H U^\dagger(\mathbf{k})$  becomes

$$\tilde{H} = \frac{\hbar^2 k^2}{2m} \left( \gamma_1 + \frac{5}{2} \gamma_2 - 2\gamma_2 S_z^2 \right) + U(\mathbf{k}) V(\mathbf{x}) U^\dagger(\mathbf{k}) \quad (3)$$

Eigenvalues of  $S_z$  physically describe the helicity  $\lambda = \hbar^{-1} \mathbf{k} \cdot \mathbf{S} / k$  in the original basis. The kinetic part  $H_0$  now becomes diagonal, in the representation where  $S_z$  is diagonal. Because  $\mathbf{x} = i\partial_{\mathbf{k}}$ , the potential term becomes  $V(\tilde{\mathbf{D}})$ , where the covariant derivative  $\tilde{\mathbf{D}}$  is defined by  $\tilde{\mathbf{D}} = i\partial_{\mathbf{k}} - \tilde{\mathbf{A}}$  and  $\tilde{\mathbf{A}} = -i U(\mathbf{k}) \partial_{\mathbf{k}} U^\dagger(\mathbf{k})$ . Because  $\tilde{\mathbf{A}}$  is a pure gauge potential, there is no curvature associated with it. Up to this point, the transformation is exact. We now consider adiabatic transport and make a corresponding approximation. As is usually assumed in the transport theory, we neglect the interband transitions, i.e., the off-block-diagonal matrix elements of  $\tilde{\mathbf{A}}$  connecting the LH and HH bands. Then we arrive at a nontrivial adiabatic gauge connection  $\mathbf{A}$  [supporting online material (SOM) text], which takes a block-diagonal form in the LH and HH sub-space. Because each band is twofold degenerate, the gauge connection is, in general, non-Abelian. However,  $\mathbf{A}$  has no matrix elements connecting the  $\lambda = 3/2$  and  $\lambda = -3/2$  states in the HH band, because the gauge field  $\tilde{\mathbf{A}}$  only connects states with helicity difference  $\Delta\lambda = 0, \pm 1$ . Therefore, the non-Abelian structure is only present in the LH band. For simplicity of presentation, we shall first make an additional, Abelian approximation (AA),

<sup>1</sup>Department of Applied Physics, University of Tokyo, Hongo, Bunkyo-ku, Tokyo 113-8656, Japan. <sup>2</sup>Correlated Electron Research Center (CERC), National Institute of Advanced Industrial Science and Technology (AIST), Tsukuba Central 4, Tsukuba 305-8562, Japan. <sup>3</sup>CREST, Japan Science and Technology Corporation (JST). <sup>4</sup>Department of Physics, McCullough Building, Stanford University, Stanford CA 94305-4045, USA.

\*To whom correspondence should be addressed. E-mail: murakami@appi.t.u-tokyo.ac.jp

in which only the diagonal components in  $\mathbf{A}$  are retained. Afterward, we shall give our final results, including fully the non-Abelian corrections.

Within the AA,  $\mathbf{A}$  is a diagonal 4 by 4 matrix in the helicity basis. Because a band-touching point acts as a Dirac magnetic monopole in momentum space (6), each diagonal component of  $\mathbf{A}(\mathbf{k})$  is given by that of a Dirac monopole at  $\mathbf{k} = 0$ , with the monopole strength  $eg$  given by  $\lambda$ . The associated field strength is given by

$$F_{ij} \equiv i[D_i, D_j] = \epsilon_{ijk} \lambda \frac{k_k}{k^3} \quad (4)$$

The effective Hamiltonian takes the form

$$H^{\text{eff}} = \frac{\hbar^2 k^2}{2m_\lambda} + V(\mathbf{x}). \quad (5)$$

Henceforth,  $x_i$  denotes a covariant derivative in momentum space:  $x_i = D_i = i\partial/\partial k_i - A_i(\mathbf{k})$ . The definition of  $x_i$  has changed by projecting the original Hamiltonian  $H$  onto the HH or LH band. Whereas  $H^{\text{eff}}$  seems to be trivial, its nontrivial dynamics are revealed through the nontrivial commutation relations

$$[k_i, k_j] = 0, [x_i, k_j] = i\delta_{ij}, [x_i, x_j] = -iF_{ij}. \quad (6)$$

Such a situation also happens in the Gutzwiller projection of the SO(5) model (7). It also resembles the nontrivial commutation relation between the position operators of a two-dimensional electron gas projected onto the lowest Landau level (8), where  $F_{ij} = B\epsilon_{ij}$ , and  $B$  is the external magnetic field. This general algebraic structure, called “noncommutative geometry,” also underlies the four-dimensional QHE model (4). In our present context, the non-commutativity between the three-dimensional coordinates arises from the magnetic monopole in momentum space, and it is a natural generalization of the QHE to three dimensions.

The equation of motion for holes can be derived easily from Eqs. 5 and 6 as

$$\hbar \dot{k}_i = eE_i, \dot{x}_i = \frac{\hbar k_i}{m_\lambda} + F_{ij} \dot{k}_j \quad (7)$$

The last term, proportional to  $F_{ij}$ , is a topological term, describing the effect of the magnetic monopole on the orbital motion. It represents a “Lorentz force” in momentum space, making the hole velocity noncollinear with its momentum, in contrast to the usual situations. In fact, if we interchange the roles of  $x$  and  $k$  in this term, this term becomes the Lorentz force for a charged particle moving in the presence of a magnetic monopole in real space. This set of equations can be integrated analytically (SOM text), and the resulting trajectory is shown in Fig. 2. The hole motion in real space obtains a shift perpendicular to  $\mathbf{S}$ . This shift is analogous to the deflection of a charged particle by a magnetic

monopole in a direction perpendicular to the plane spanned by its position and velocity vectors (9). It causes a spin current perpendicular to both  $\mathbf{E}$  and  $\mathbf{S}$ . For example, for  $\mathbf{E}$  parallel to the  $+z$  direction, the spin current for each band at zero temperature, with spin parallel to the  $x$  axis, flowing to the  $y$  direction is given by

$$j_y^x = \frac{eE_z}{36\pi^2} (9k_F^H + k_F^L) \quad (8)$$

which is obtained by summing contributions from all the filled states. Here, we assumed that the equilibrium momentum distribution is attained by the random impurity scattering that causes the charge relaxation. Eq. 7 describes only the ballistic motion, and scattering by random impurities would lead to additional contributions to the spin current. As one can see from the detailed discussions in the SOM text, these extrinsic effects are not only small, but also scale with a higher power of  $k_F \sim n^{1/3}$ , where  $n$  is the hole density. Therefore, by plotting  $\sigma_y/n^{1/3}$  against  $n$  and

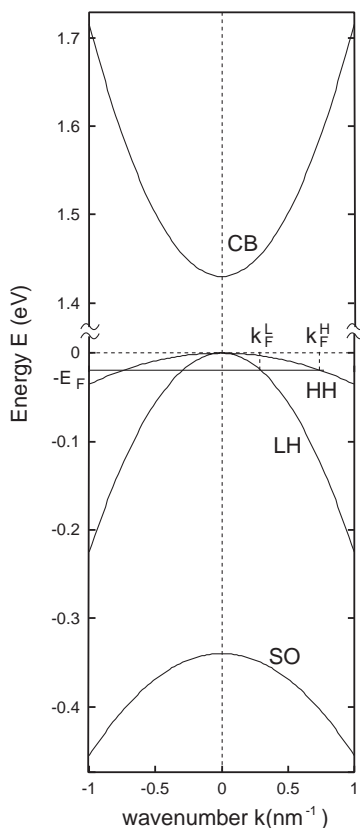


**Fig. 1.** Approximate band structure of GaAs. We neglect the small splitting due to inversion symmetry breaking. We also neglect the anisotropy of the bands. The conduction band (CB) is twofold degenerate. The valence bands consist of the HH, the LH, and the split-off (SO) bands, each of which is twofold degenerate. We consider the p-GaAs, and the Fermi momentum for each band is labeled as  $k_F^H$  and  $k_F^L$ , respectively. The Fermi energy shown corresponds to  $n = 10^{19} \text{ cm}^{-3}$ .

extrapolating to the limit of  $n \rightarrow 0$ , the constant intercept would uniquely determine our predicted dissipationless spin conductivity.

It is worth noting that this AA becomes exact in zero-gap semiconductors, e.g.,  $\alpha$ -Sn. In this class of materials, the bottom of the conduction band and the top of the valence band correspond to the LH and HH bands in other semiconductors like GaAs. These two bands touch at  $\mathbf{k} = 0$ . In this case, p-doping introduces holes only into the HH band, and the AA becomes exact.

The spin current induced by the electric field can also be understood in terms of the conservation of the total angular momentum  $\mathbf{J} = \hbar \mathbf{x} \times \mathbf{k} + \mathbf{S}$ . As remarked earlier,  $\mathbf{J}$  commutes with  $H_0$ . When  $\mathbf{E}$  is parallel to the  $z$  direction,  $J_z$  also commutes with the potential. Therefore, substituting  $\mathbf{S} = \lambda \hbar \hat{\mathbf{k}} = \lambda \hbar \mathbf{k}/k$ , we obtain

$$J_z = \hbar(\dot{\mathbf{x}} \times \mathbf{k})_z + \hbar(\mathbf{x} \times \dot{\mathbf{k}})_z + \lambda \hbar \dot{k}_z = 0 \quad (9)$$

The second term, representing the torque, vanishes in our case because  $\mathbf{k}$  points along the  $z$  direction. The first term  $\hbar(\dot{\mathbf{x}} \times \mathbf{k})_z$  vanishes in usual problems; however, it does not in our case, due to the noncollinearity of the velocity and the momentum. Furthermore, the first term, describing the time derivative of the orbital angular momentum  $\mathbf{L} = \hbar \mathbf{x} \times \mathbf{k}$ , is proportional to the spin current. The third term  $\lambda \hbar \dot{k}_z$ , describing the time derivative of the spin angular momentum  $\mathbf{S}$ , can be easily evaluated from the acceleration equation in Eq. 7. Therefore, we see that the conservation of the total angular momentum in Eq. 9 directly implies the spin current in Eq. 8. The spin current flows in

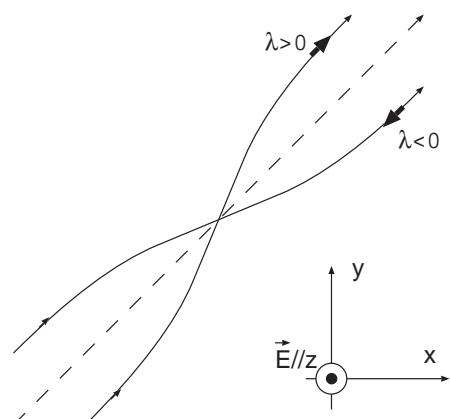


**Fig. 2.** The real-space trajectory of the hole obtained by solving Eq. 7. The electric field  $\mathbf{E} = e^{-1}\nabla V$  is parallel to the  $+z$  direction. Due to the noncommutative relation between the components of the position operator  $x_i$ , i.e.,  $[x_i, x_j] = -iF_{ij}$ , with  $F_{ij}$  being the gauge curvature defined in the momentum space, the hole obtains a transverse velocity whose direction depends on the helicity  $\lambda = \hbar^{-1} \mathbf{k} \cdot \mathbf{S}/k$ , indicated by the thick arrows. The broken line is parallel to  $\mathbf{k}$ .

## REPORTS

such a way that the change of  $\mathbf{L}$  exactly cancels the change of  $\mathbf{S}$ .

We now discuss the correction due to the non-Abelian nature of the gauge connection of the LH band. Remarkably, even though the gauge connection is non-Abelian, the associated field strength is Abelian and gives a correction factor of  $-3$ , compared with the AA (10–12). The equation of motion modified accordingly agrees with that obtained by generalizing the wave packet formalism (13) to the non-Abelian case. This non-Abelian correction gives the following result for the spin current:

$$j_y^x = \frac{eE_z}{12\pi^2} (3k_F^H - k_F^L) = \frac{\hbar}{2e} \sigma_s E_z \quad (10)$$

Here, we defined  $\sigma_s$  to have the same dimension as the electrical conductivity, to facilitate comparison. The spin current equation is rotationally invariant, with the covariant form given in Eq. 1, and is the central result of our paper. In contrast with similar effects (14, 15), this spin current has a topological character; the spin conductivity  $\sigma_s$  in Eq. 1 is independent of the mean free path and relaxational rates, and all states below the Fermi energy contribute to the spin current, where each contribution is determined purely by the gauge curvature in momentum space, similar to the QHE (3). Assuming the hole density  $n = 10^{19} \text{ cm}^{-3}$ , the mobility of the holes at room temperature in GaAs is  $\mu = 50 \text{ cm}^2/\text{V}\cdot\text{s}$  (16), and the conductivity is  $\sigma = en\mu = 80 \Omega^{-1} \text{ cm}^{-1}$ . On the contrary, the spin Hall conductivity  $\sigma_s$  in Eq. 10 is estimated as  $\sigma_s \sim 80 \Omega^{-1} \text{ cm}^{-1}$ , being of the same order with  $\sigma$ . For lower carrier concentration,  $\sigma_s$  becomes larger than  $\sigma$ ; for  $n = 10^{16} \text{ cm}^{-3}$ , we have  $\sigma = 0.6 \Omega^{-1} \text{ cm}^{-1}$  and  $\sigma_s = 7 \Omega^{-1} \text{ cm}^{-1}$ . At finite temperature, Eq. 10 is modified only through the Fermi distribution function  $n^{\uparrow}(\mathbf{k})$ . Because the typical energy difference between the LH and HH bands at the same wavenumber is about 0.1 eV, which largely exceeds the energy scale of the room temperature  $\sim 0.025 \text{ eV}$ , our predicted effect remains of the same order even at room temperature.

The nondissipative spin transport equation Eq. 1 does not violate the time-reversal symmetry  $T$ . Our microscopic Hamiltonian  $H$ , the electric field  $\mathbf{E}$ , and the spin current are all  $T$  invariant. Therefore, the electric field and the spin current can be related by a  $T$  symmetric, dissipationless transport coefficient  $\sigma_s$ . This situation is to be contrasted with Ohm's law. As the charge current is odd under  $T$ , while the electric field is even, they can only be related by a  $T$  antisymmetric, dissipative transport coefficient, namely, the charge conductivity. One of the main objectives in quantum computing is to achieve reversible computation (17, 18). From the above analysis, we see that there is a fundamental difference between the ordinary irreversible electronics computation based on Ohm's law and the reversible spintronics computation based on Eq. 1. The time reversal symmetry property encoded in Eq. 1 could provide a fundamental principle for the reversible quantum computation.

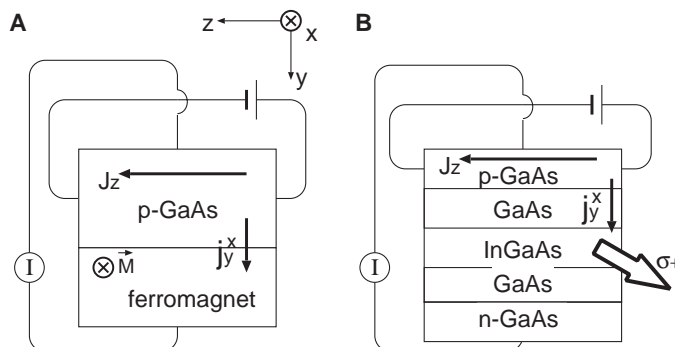
This spin current is also useful for spin injection into semiconductors. Although effective spin injection is necessary for spintronic devices, it has been an elusive issue (2). Usage of ferromagnetic metals is not practical because most of the spin polarizations are lost at the interface due to conductivity mismatch between metal and semiconductor (19, 20). Spin injection from ferromagnetic semiconductors such as  $\text{Ga}_{1-x}\text{Mn}_x\text{As}$  has been successful (21–23). Nevertheless,  $T_c$  is at most 110 K for  $\text{Ga}_{1-x}\text{Mn}_x\text{As}$ , still too low for practical use at room temperature. Thus, it is desirable to find an effective method for spin injection. The electric field-induced spin current serves as a spin injector, because it creates a spin current inside the semiconductor. One might worry that the short relaxation time  $\tau_s \sim 100 \text{ fs}$  (24) of the hole spins. This shortness of  $\tau_s$  is because the strong spin-orbit interaction in the valence band combines the relaxation of momenta and spins (25). Most of the efforts on the spintronics in GaAs have been focused on electrons in the conduction bands, which have much

longer spin-relaxation time ( $\sim 100 \text{ ps}$ ) (26). Nevertheless, our spin current is free from such rapid relaxation of spins of holes, because it is a purely quantum mechanical effect with equilibrium spin-momentum distribution. Only when the spin-momentum distribution deviates from equilibrium, e.g., in spin accumulation at boundaries of the sample, does the rapid relaxation of hole spins become effective.

One can consider following experimental setups for detection of the constant spin supply from p-GaAs. When the electric field is applied along the  $z$  direction and the electric current  $J_z$  is induced, the  $s^x$  spin current  $j_y^x$  will flow along the  $y$  direction. One possibility is to see the spin-dependent electric transport through a ferromagnetic electrode with the magnetization  $\mathbf{M}$  along  $\pm x$  direction attached to the positive  $y$  side of the sample. With a lead connecting this electrode and the other (negative  $y$ ) side of p-GaAs as shown in Fig. 3A, one should see a change of the electric current  $I$  depending on the direction of  $\mathbf{M}$ . The ratio of  $I$  when  $\mathbf{M}$  is along  $\pm x$ -direction,  $I(+x)/I(-x)$ , is expected to be well larger than unity. For the ferromagnetic electrode, ferromagnetic metals are not efficient because of the conductance mismatch (20). Instead, ferromagnetic semiconductors will be suitable. Another possibility is to measure circular polarization of light emitted via recombination with electrons. This can be achieved by a similar experimental setup in (21), replacing (Ga,Mn)As by p-GaAs, where the quantum well structure of (In,Ga)As is sandwiched by p-GaAs and n-GaAs (Fig. 3B). The spin current injected along the  $y$  direction will be recombined with the electrons supplied from the n-GaAs in the (In,Ga)As quantum well.

When the system is not connected to the leads along the  $y$  direction, spins accumulate near the edges of the sample. This spin polarization can, in principle, be measured by the Kerr rotation. The spin distribution is determined by a balance between the spin current supply and the spin relaxation. At room temperature, because  $\tau_s = 100 \text{ fs}$  (24) is rather short, the area density of spin accumulation at the sample surface,  $j_y^x \tau_s$ , is too small to be observed. However, there are several ways to make  $\tau_s$  longer. One is to lower the temperature. Another is to inject the spin into n-GaAs through the p-n junction, as demonstrated recently (27, 28). The spin lifetime of electrons in GaAs is 100 ps,  $10^3$  times longer than that of holes. Thereby, the spin current can be detected by the Kerr rotation through surface reflection.

**Fig. 3.** Experimental setups for the detection of spin current induced by an electric field. (A) Detection by attaching a ferromagnetic electrode. The dependence of current  $I$  flowing into the electrode on the direction of the magnetization  $\mathbf{M}$  is to be measured. (B) Detection by measuring the polarization of the emitted light in the quantum well of (In,Ga)As. The emitted light with circular polarization is shown as an open arrow. Right and left circular polarization will be switched when the direction of the external electric field is reversed.



### References and Notes

1. G. A. Prinz, *Science* **282**, 1660 (1998).
2. S. A. Wolf *et al.*, *Science* **294**, 1488 (2001).
3. D. J. Thouless, M. Kohmoto, M. P. Nightingale, M. Den Nijs, *Phys. Rev. Lett.* **49**, 405 (1982).



4. S.-C. Zhang, J.-P. Hu, *Science* **294**, 823 (2001).
5. J. M. Luttinger, *Phys. Rev.* **102**, 1030 (1956).
6. M. V. Berry, *Proc. R. Soc. London A* **392**, 45 (1984).
7. S.-C. Zhang, J.-P. Hu, E. Arrigoni, W. Hanke, A. Auerbach, *Phys. Rev. B* **60**, 13070 (1999).
8. P. Prange, S. M. Girvin, *The Quantum Hall Effect* (Springer, Berlin, 1997).
9. J. D. Jackson, *Classical Electrodynamics* (Wiley, New York, 1998).
10. A. Zee, *Phys. Rev. A* **38**, 1 (1988). Note that there is a misprint in this reference; in the left column of page 2, the field strength should be  $F = imd\Omega$ .
11. D. P. Arovas, Y. Lyanda-Geller, *Phys. Rev. B* **57**, 12302 (1998).
12. T. Jungwirth, Q. Niu, A. H. MacDonald, *Phys. Rev. Lett.* **88**, 207208 (2002).
13. G. Sundaram, Q. Niu, *Phys. Rev. B* **59**, 14915 (1999).
14. J. E. Hirsch, *Phys. Rev. Lett.* **83**, 1834 (1999).
15. E. N. Bulgakov, K. N. Pichugin, A. F. Sadreev, P. Štréda, P. Šeba, *Phys. Rev. Lett.* **83**, 376 (1999).
16. Landolt-Börnstein: *Numerical Data and Functional Relationships in Science and Technology—New Series, Group III, Volume 17, Subvolume a*, O. Madelung, Ed. (Springer, Berlin, 1982).
17. R. P. Feynman, A. J. G. Hey, R. W. Allen, *Feynman Lectures on Computation* (Westview Press, Boulder, CO, 2000).
18. D. Loss, D. P. DiVincenzo, *Phys. Rev. A* **57**, 120 (1998).
19. P. R. Hammar, B. R. Bennett, M. J. Yang, M. Johnson, *Phys. Rev. Lett.* **83**, 203 (1999).
20. G. Schmidt, D. Ferrand, L. W. Molenkamp, A. T. Filip, B. J. van Wees, *Phys. Rev. B* **62**, R4790 (2000).
21. Y. Ohno *et al.*, *Nature* **402**, 790 (1999).
22. R. Fiederling *et al.*, *Nature* **402**, 787 (1999).
23. R. Mattana *et al.*, *Phys. Rev. Lett.* **90**, 166601 (2003).
24. D. J. Hilton, C. L. Tang, *Phys. Rev. Lett.* **89**, 146601 (2002).
25. F. Meier, B. P. Zakharchenya *Optical Orientation* (North Holland, Amsterdam, 1984).
26. Y. Ohno, R. Terauchi, T. Adachi, F. Matsukura, H. Ohno, *Phys. Rev. Lett.* **83**, 4196 (1999).
27. E. Johnston-Halperin *et al.*, *Phys. Rev. B* **65**, 041306 (2002).
28. M. Kohda, Y. Ohno, K. Takamura, F. Matsukura, H. Ohno, *J. Supercond.* **16**, 167 (2003).
29. We thank C. Herring and M. Gonokami for helpful discussions. This work is supported by Grant-in-Aids from the Ministry of Education, Culture, Sports, Science and Technology of Japan; the NSF under grant number DMR-9814289; and the U.S. Department of Energy, Office of Basic Energy Sciences under contract DE-AC03-76SF00515.

## Supporting Online Material

www.sciencemag.org/cgi/content/full/1087128/DC1

SOM Text

References

22 May 2003; accepted 25 July 2003

Published online 7 August 2003;

10.1126/science.1087128

Include this information when citing this paper.

## Preparing Protein Microarrays by Soft-Landing of Mass-Selected Ions

Zheng Ouyang,<sup>1</sup> Zoltán Takáts,<sup>1</sup> Thomas A. Blake,<sup>1</sup>  
Bogdan Gologan,<sup>1</sup> Andy J. Guymon,<sup>1</sup> Justin M. Wiseman,<sup>1</sup>  
Justin C. Oliver,<sup>2</sup> V. Jo Davisson,<sup>2</sup> R. Graham Cooks<sup>1\*</sup>

Intact, multiply protonated proteins of particular mass and charge were selected from ionized protein mixtures and gently landed at different positions on a surface to form a microarray. An array of cytochrome c, lysozyme, insulin, and apomyoglobin was generated, and the deposited proteins showed electrospray ionization mass spectra that matched those of the authentic compounds. Deposited lysozyme and trypsin retained their biological activity. Multiply charged ions of protein kinase A catalytic subunit and hexokinase were also soft-landed into glycerol-based liquid surfaces. These soft-landed kinases phosphorylated LRRASLG oligopeptide and D-fructose, respectively.

Patterning of biological macromolecules onto surfaces in the form of microarrays (“chips”) produces a sample format suited to automated analysis for biological activity (1–4). The archetypal case is the widely used DNA chip, where a high spot density (10,000 spots/cm<sup>2</sup>) is created by automated procedures that supply the constituent nucleotides to preselected positions. It is widely expected that the development of proteomics and the application of combinatorial chemistry methods in drug discovery will mandate similar sample formats for studies of proteins and other biological compounds. Techniques developed for deposition of macromolecules onto solid supports include microdispensing (5), electrospray deposition (6), robotic printing (7), stamping (8), and ink jet deposition (9).

Ion soft-landing is another method with potential value in chip production (10). The

soft-landing of molecular ions onto surfaces, first proposed (11) in 1977, was later demonstrated (12) with low-kinetic energy (typically 5 to 10 eV) mass-selected ion beams at polyfluorinated self-assembled monolayer (SAM) surfaces. Mass spectrometric analysis was used to confirm the presence of sterically bulky soft-landed organic ions such as *N,N*-dimethylisothiocyanate. Simple organic cations (13, 14) and a 16-nucleotide double-stranded DNA (15) (mass ~ 10 kD) have also been soft-landed intact onto surfaces, as have metal clusters (16). In some of these cases there is evidence that the molecular entity on the surface is the ion (12); in others, it is the corresponding neutral molecule. In one striking experiment, virus particles were ionized, crudely mass-selected in a time-of-flight instrument, and showed evidence of activity after deposition on a collector plate (17).

The use of mass spectrometry as a separation method is expected to provide high selectivity because components having different molecular formulae, including isotopomers, can be separated and individually soft-landed. This should include separate gly-

coforms of proteins, individual polysulfonated forms, and other posttranslationally modified variants [the mass difference due to acetylation of an immunoglobulin G antibody can be resolved with a mass resolution of 3000]. In principle, too, the technique should exhibit good spatial resolution because ion beam spots of micrometer dimensions are attainable. Potential disadvantages are the relatively small amounts of ionized material and the possibility of alteration of delicate biological molecules in the course of ionization, mass analysis, or soft-landing.

To investigate the possibility of soft-landing of mass-selected multiply charged protein ions, we ionized mixtures of up to four well-studied proteins—cytochrome c, lysozyme, insulin, and apomyoglobin (18)—by electrospray ionization (ESI). The proteins were selected individually by mass/charge ratio (*m/z*) and deposited onto various surfaces (19, 20). The experiments were performed with two instruments: a commercial SSQ-710C (Thermo Finnigan, San Jose, California) quadrupole mass spectrometer that was modified by addition of a surface and its surface moving stage and a custom-built instrument that used a Thermo Finnigan linear ion trap (LIT) (21) shown in Fig. 1. This latter instrument includes an ESI ion source, a high-capacity LIT, wave form capabilities for ion isolation, a radial detector for mass analysis, and facilities for low-energy transfer of trapped, mass-selected ions onto specific spots on an electronically movable target. In comparison with the SSQ instrument, the LIT provides considerably higher ion flux (on the order of 10<sup>9</sup> to 10<sup>10</sup> s<sup>-1</sup>), the opportunity to check the spectrum of the material to be landed by *in situ* mass analysis, and more control over the landing energy. The landed proteins were redissolved into a methanol/water (1:1) rinse solution. The rinse solutions were examined by ESI with an LCQ Classic mass spectrometer (Thermo Finnigan). In separate experiments, matrix-assisted laser desorption ionization (MALDI) was used to examine the deposited proteins *in situ* (22).

<sup>1</sup>Department of Chemistry, <sup>2</sup>Department of Medicinal Chemistry and Molecular Pharmacology, Purdue University, West Lafayette, IN 47907, USA.

\*To whom correspondence should be addressed. E-mail: cooks@purdue.edu